Structural and dynamical properties of densely packed glass-forming $Ni_{66.7}B_{33.3}$

S. Nell,[1,*] F. Yang,[1] D. Holland-Moritz,[1] Th. Voigtmann,[1,2] J. Hu,[1] T. C. Hansen,[3] T. Buslaps,[4] and A. Meyer[1,3]

[1]*Institut für Materialphysik im Weltraum, Deutsches Zentrum für Luft- und Raumfahrt (DLR), 51170 Köln, Germany*

[2]*Theoretische Physik, Heinrich-Heine-Universität Düsseldorf, 40225 Düsseldorf, Germany*

[3]*Institut Laue-Langevin - BP156, 38042 Grenoble Cedex 9, France*

[4]*European Synchrotron Radiation Facility, 71 Avenue des Martyrs, 38000 Grenoble, France*

(Received 9 January 2024; accepted 18 June 2024; published 22 July 2024)

We investigate the structure-dynamics relation of the densely packed, glass-forming $Ni_{66.7}B_{33.3}$ melt using a combination of neutron diffraction and isotopic substitution as well as x-ray diffraction. By additionally utilizing the containerless experimental method of electrostatic levitation, we were able to obtain partial structure factors of high precision. Self- and interdiffusion coefficients were calculated by using the measured partial structure factors as an input for the mode-coupling theory of the glass transition. These are in qualitative agreement with experimentally measured results for liquid $Ni_{66.7}B_{33.3}$. Despite a similar packing density in $Zr_{64}Ni_{36}$, it is found that the calculated diffusivities D_{Ni} and D_B in $Ni_{66.7}B_{33.3}$ differ from each other by a factor of 2. However, the Darken approximation for the relation of self- and interdiffusion is applicable for the $Ni_{66.7}B_{33.3}$ melt.

DOI: 10.1103/PhysRevB.110.014206

I. INTRODUCTION

One central goal of understanding transport phenomena in liquid matter is to establish relations between dynamical and structural properties on an atomic scale. For crystalline solids, such structure-property relations reveal well-known diffusion mechanisms, e.g., via interstitials or vacancies [1]. In liquids, the prevailing mechanisms of diffusion are less clear due to their disordered structure. Nevertheless, the atomic dynamics here are also governed by the interplay of topological (TSRO) and chemical short range order (CSRO) [2–6].

For simple metallic liquids like alkali metals, a number of early models have been developed based on kinetic theory, with a transport mechanism of random, uncorrelated binary collisions, which results in semiempirical relations between dynamics and thermodynamic parameters of the melt [7,8]. These kinetic theory models apply only phenomenologically and the physical meaning of the parameters is unclear. In particular, for more densely packed, glass-forming melts, contributions of collective effects on melt kinetics become increasingly important [5,6,9–12]. As an indication, deviations from the Stokes-Einstein relation (SER) are observed for such glass-forming melts, where the self-diffusion coefficient and the melt viscosity exhibit the same temperature dependence [5,9].

One possibility to directly link the structure and the atomic dynamics of densely packed melts is provided by the mode-coupling theory of the glass transition (MCT) [13,14], which makes predictions of dynamic quantities using (partial) structure factors of the liquid as an input [15]. These (partial) structure factors define the coupling coefficients of MCT. A metallic glass-forming alloy system, which has been subject to a large number of investigations on this topic, is Zr-Ni [11,16,17]. MCT predicts practically identical self-diffusion coefficients for Ni and Zr in the $Zr_{64}Ni_{36}$ alloy, and thus strongly coupled self-diffusion coefficients [16] in $Zr_{64}Ni_{36}$. For $Zr_{64}Ni_{36}$, the Onsager coefficient is considerably lower than predicted by the Darken equation, which means that Darken is not valid here [16]. Moreover, also the prediction of similar Zr and Ni self-diffusion, as well as the interdiffusion coefficients can be confirmed by tracer and interdiffusion measurements [11,18]. It can be shown for $Zr_{64}Ni_{36}$ that this is a result of the structurally preferred Zr-Ni nearest-neighbor pairs, and a dominant, slow kinetic contribution to the interdiffusion. Similar results were reported for melts of Hf-Ni alloys [19].

One aspect that decisively influences the atomic structure and the dynamics are the atomic interactions and the bonding character (metallic or covalent). Melts of pure transition metals like Ni, Fe, Zr, Ti, or Cu are characterized by an icosahedral short-range order (SRO) and coordination numbers of about 12 [20–22]. Such an icosahedral short range was already predicted in 1950 by Frank for monoatomic metallic melts under the assumption of Lennard-Jones-like interactions of spherical symmetry [23]. A more covalent bonding character may lead to directional bonding, strongly influencing the short-range order. For instance, melts of pure B [24], Si [25], or Ge [26] show short-range structures characterized by coordination numbers of roughly 6. The considerably lower density of packing of liquid Ge results in a faster atomic dynamics as compared to the densely packed metallic melts [26]. For alloy melts, the situation is even more complex. In addition to the bonding nature, the atomic size ratio of the components will also decisively influence the short-range order. Some degree of directional bonding cannot be ruled out even for alloy melts consisting of purely metallic elements. For Cu-Ni melts that consist of chemically similar elements of similar atomic radius, again an icosahedral short-range order was observed [22]. Nevertheless, for Zr-Ni,

*Contact author: sarah.nell@dlr.de

Hf-Ni, Zr-Cu, or Nb-Ni melts, other types of short-range order are observed that are characterized by coordination numbers higher than 12 [17,27]. First-principles molecular dynamics simulations of Zr_2TM (TM= Ag, Co, Cu, Ni) melts suggest that both the atomic size ratio as well as a certain degree of directional bonding from interactions between the d electrons of the Zr and TM atoms determine the short-range order of these liquids [28]. For alloys containing metalloids, even stronger influences of covalent bonding may be expected. For some metal-metalloid glasses, like Pd-Si of Pd-Ni-P, a short-range order consisting of trigonal prismatic configurations is suggested to be induced by covalentlike bonds between the metalloids and the transition metals [29,30]. For Zr-Co-Al melts, a p-d hybridization between the transition metals and the post-transition melt Al that is often considered as metalloidlike was observed by nuclear magnetic resonance investigations [31]. This results in a shortening of the bond lengths and the formation of stringlike structures of Co and Al atoms. These hybridization effects provide an explanation of the slowdown of the atomic dynamics of the melts [3] and the enhancement of the glass-forming ability by addition of Al.

Here, we report on the metallic glass forming alloy $Ni_{66.7}B_{33.3}$, which has a similar packing fraction, as well as almost identical Ni self-diffusion coefficients and melt viscosities as $Zr_{64}Ni_{36}$ [5]. $Ni_{66.7}B_{33.3}$ also shows a similar deviation from the SER as observed in the $Zr_{64}Ni_{36}$ melt, indicating the collective nature of the mass transport in the melt [5]. However, Ni-B also exhibits distinct differences when compared to the Zr-Ni system: boron is a nonmetallic constituent with a considerably smaller atomic size than Ni (covalent radii: $r_B = 0.80$ Å, $r_{Ni} = 1.15$ Å [32]). This raises the question whether these differences also influence the dynamical features of the system concerning interdiffusion and how the transport coefficients are affected by the atomic size ratio and chemical short-range order. Since the measurement of the interdiffusion coefficients is not trivial, we used MCT to give a qualitative prediction of the dynamics of the investigated liquid alloy $Ni_{66.7}B_{33.3}$. By studying the partial structure factors of the $Ni_{66.7}B_{33.3}$ alloy, MCT calculation predicts a more decoupled dynamics between Ni and B compared to that of $Zr_{64}Ni_{36}$, as well as a kinetic contribution to the interdiffusion according to Darken's equation. This can be attributed to the small B atoms, and is confirmed by the experimentally determined interdiffusion coefficient.

II. EXPERIMENTAL DETAILS

For determining the partial structure factors of the liquid $Ni_{66.7}B_{33.3}$ alloy, measurements with the necessary three different scattering contrasts were achieved by combining neutron diffraction with isotopic substitution and high energy x-ray diffraction (XRD). Neutron diffraction experiments have been performed at the high-intensity two-axis diffractometer D20 of the Institut Laue-Langevin (ILL) [33] in Grenoble on $Ni_{66.7}B_{33.3}$ by using two different Ni isotopes: natural Ni and ^{60}Ni. In addition, because natural boron has a high neutron absorption cross section ($\sigma_{abs} = 767$ barn [34]), the samples for the neutron diffraction experiments were all synthesized with the isotope ^{11}B ($\sigma_{abs} = 0.0055$ barn [34]). This was alloyed with natural Ni or ^{60}Ni by arc melting these constituents under a high purity Ar-atmosphere (purity 99.9999%).

During the diffraction experiments, the samples were processed using the containerless technique of electrostatic levitation utilizing the same facility as that described in Ref. [35]. This avoids reactions between the liquid samples and a container at elevated temperature. At the same time, it is possible to access the undercooled liquid state by avoiding of heterogeneous nucleation at crucible walls. The absence of container materials in the vicinity of the sample also allows structure factors to be measured with an excellent signal-to-background ratio.

An incoming neutron wavelength of 0.94 Å gives access to a momentum transfer q of up to 13 Å^{-1}, which is a good compromise between neutron flux and the accessible q range. The typical sample mass used was about 450 mg, and the samples were all processed under a high vacuum environment (10^{-6} mbar). To derive the liquid structure factor, the measured raw intensity was corrected for the background from the empty electrostatic levitator, for sample self-absorption and for the effect of inelastic scattering, normalized to a vanadium standard, also taking multiple scattering into account. A more detailed description of the data treatment procedure can be found in Ref. [36].

A third independent scattering contrast for deriving the partial structure factors was obtained by high energy x-ray diffraction. The experiments were carried out at the ID15A (EH2) beam line at the European Synchrotron Radiation Facility (ESRF) [37]. The measurement was performed in a similar electrostatic levitation setup as that used in the neutron diffraction experiments, only the sample mass is smaller, on the order of about 110 mg. The measurements were done in transmission geometry with monochromatic synchrotron radiation of 100 keV energy. A PerkinElmer Flat panel detector (pixel size 200 μm, total area 40 cm × 40 cm) was placed at 720 mm distance downstream from the sample to collect 2D diffraction patterns. The maximum accessible momentum transfer q is about 15 Å^{-1}. Diffractograms of the $Ni_{66.7}B_{33.3}$ liquid were recorded with an exposure time of 0.5 s during cooling of the sample until crystallization of the levitated droplet set in. Intensity spectra $I(q)$ were integrated from the two-dimensional detector images using the PYFAI software package [38], with a calibration of the sample-detector distance using a CeO_2 standard and a correction of the detector dark current. The total structure factors $S(q)$ are calculated from $I(q)$ using the PDFGETX2 [39] analysis software after subtracting of the empty levitation chamber contribution, correcting for self-absorption, Compton scattering, multiple scattering, polarization, and oblique incidence.

The MCT is a fertile tool to relate the structure of a liquid alloy with its dynamics by giving qualitative predictions of the dynamics. It solves the equation of motion provided according to the partial Zwanzig-Mori formalism for the partial density correlation functions $\boldsymbol{S}(q,t) = \langle \rho_q(t)^* \rho_q \rangle$ of an isotropic, transitionally invariant system,

$$\ddot{\boldsymbol{S}}(q,t) + \boldsymbol{\Omega}_q^2 \cdot \boldsymbol{S}(q)^{-1} \cdot \boldsymbol{S}(q,t) + \int_0^t \boldsymbol{M}_q(t-t') \cdot \dot{\boldsymbol{S}}(q,t')dt' = \boldsymbol{0}, \quad (1)$$

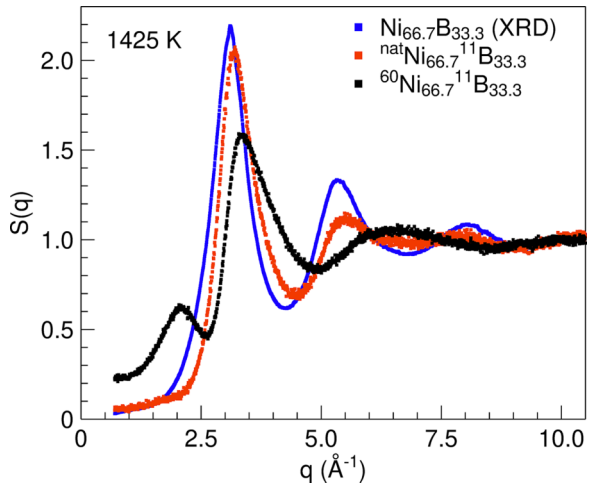

FIG. 1. Total structure factors $S(q)$ of liquid $^{60}Ni_{66.7}{}^{11}B_{33.3}$, $^{nat}Ni_{66.7}{}^{11}B_{33.3}$, and $Ni_{66.7}B_{33.3}$ (XRD) at 1425 K versus the wave number q. Symbols show the results of the neutron diffraction and x-ray diffraction measurements.

where $\mathbf{\Omega}_q$ corresponds to thermal frequencies, which govern the short-time relaxation, and $\boldsymbol{M}(q,t)$ is the so-called memory kernel, which is a nonlinear functional of the density correlation function $\boldsymbol{S}(q,t)$ [14]. For an alloy with element species α and β, the $\boldsymbol{S}(q,t)$ reads

$$S_{\alpha\beta}(q,t) = \frac{1}{N}\sum_{k_\alpha=1}^{N_\alpha}\sum_{k_\beta=1}^{N_\beta}\langle\exp\{i\vec{q}\cdot[\vec{r}_{k_\alpha}(t)-\vec{r}_{k_\beta}(0)]\}\rangle, \qquad (2)$$

where $\vec{r}_{k_\alpha}(t)$ marks the position of the particle labeled k_α at time t [13,40]. At $t=0$, these functions yield the partial static structure factors $S_{\alpha\beta}(q)$. Kinetic quantities like the self-diffusion coefficient and the interdiffusion coefficient L can be derived by the corresponding Green-Kubo integrals of the self- and distinct velocity autocorrelation functions, respectively, by solving the equation using the experimentally determined partial structure factors $S_{\alpha\beta}(q)$ that enter $S_{\alpha\beta}(q,t)$ as input.

III. RESULTS AND DISCUSSION

The total static structure factors for liquid $Ni_{66.7}B_{33.3}$ measured by neutron and x-ray diffraction are shown in Fig. 1 at a temperature of 1425 K (T_{liq} = 1398 K [41]). The difference in the curves is a result of the different scattering contrasts. In the case of $^{60}Ni_{66.7}{}^{11}B_{33.3}$, the contribution of the boron related correlation is significantly higher than that in the other $S(q)$s measured, as the scattering length of ^{60}Ni (b = 2.8 fm [34]) is relatively small compared to the scattering length of natural Ni (b = 10.3 fm [34]) or ^{11}B (b = 6.65 fm [34]). In contrast, the x-ray total structure factor is dominated by the Ni-related correlations due to the small atomic number (5 for B, 28 for Ni) and the resulting weak x-ray scattering contribution of the boron.

The partial structure factors of the $Ni_{66.7}B_{33.3}$ melts at temperatures of 1425 K and 1550 K were calculated from the three total static structure factors by using the

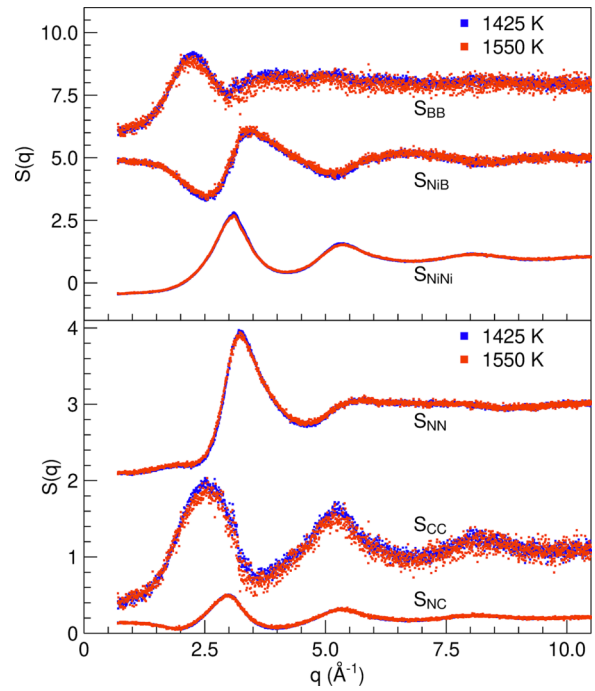

FIG. 2. Upper panel: Partial structure factors $S_{NiNi}(q)$, $S_{BB}(q)$ and $S_{NiB}(q)$ calculated using the Faber-Ziman formalism at 1425 K and 1550 K versus the wave number q. S_{NiB} and S_{BB} are shifted up along the y axis by values of 4 and 7. Lower panel: Partial structure factors $S_{NN}(q)$, $S_{CC}(q)$, and $S_{NC}(q)$ calculated using the Bathia-Thornton formalism at 1425 K and 1550 K versus the wave number q. Curves are shifted up along the y axis, S_{CC} by values of 0.1, S_{NC} by 0.2, and S_{NN} by 2.

Faber-Ziman [42],

$$S(q)^{FZ} = \frac{c_{Ni}^2\overline{b_{Ni}}^2}{\overline{b^2}}S_{NiNi}(q) + \frac{c_B^2\overline{b_B}^2}{\overline{b^2}}S_{BB}(q) + \frac{2c_{Ni}c_B\overline{b_{Ni}}\,\overline{b_B}}{\overline{b^2}}S_{NiB}(q) + 1 - \frac{\overline{b}^2}{\overline{b^2}}, \qquad (3)$$

and the Bhatia-Thornton [43],

$$S(q)^{BT} = \frac{\overline{b}^2}{\overline{b^2}}S_{NN}(q) + \frac{c_{Ni}c_B(\overline{b_{Ni}}-\overline{b_B})^2}{\overline{b^2}}S_{CC}(q) + \frac{2(\overline{b_{Ni}}-\overline{b_B})\overline{b}}{\overline{b^2}}S_{NC}(q), \qquad (4)$$

formalisms, with the concentration c and the coherent scattering length b of the atoms Ni and B ($\overline{b} = c_{Ni}\overline{b_{Ni}} + c_B\overline{b_B}$ and $\overline{b^2} = c_{Ni}\overline{b_{Ni}^2} + c_B\overline{b_B^2}$). Corresponding results are depicted in Fig. 2. The Faber-Ziman partial structure factors $S_{NiNi}(q)$, $S_{NiB}(q)$, and $S_{BB}(q)$ are shown in the upper panel of Fig. 2, which describe the different contributions of each of the atomic pairs (Ni-Ni, Ni-B, and B-B) to the total static structure factor. The lower panel shows the partial structure factors calculated using the Bhatia-Thornton formalism, where $S_{NN}(q)$ represents the topological structure of the melt, and where the CSRO is described by the partial structure factor $S_{CC}(q)$. $S_{NC}(q)$ describes the correlation between the number density and the chemical composition. The curves of $S_{CC}(q)$ show

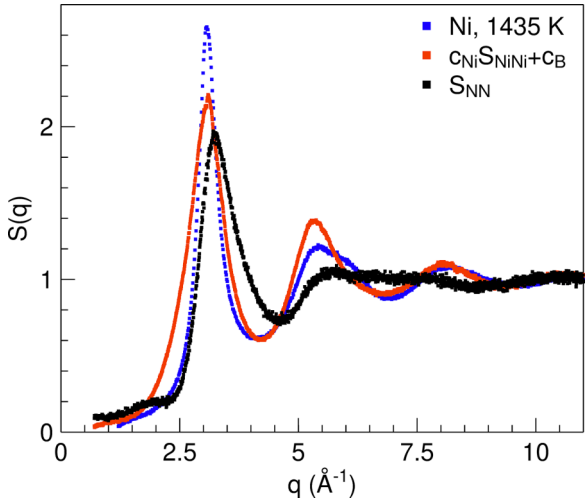

FIG. 3. Comparison of the structure factors of pure liquid Ni measured at $T = 1435$ K [20] with S_{NN} and $c_{Ni}\,S_{NiNi} + c_B$ determined here for liquid $Ni_{66.7}B_{33.3}$ at $T = 1425$ K.

strong oscillations, indicating the presence of a pronounced CSRO. When comparing the $S(q)$s at temperatures of 1425 K and 1550 K for both sets of partial structure factors, only a weak temperature dependence is observed within the measured temperature range of 125 K with the $S(q)$s measured at 1550 K showing slightly lower amplitude compared to that at 1425 K.

When alloying Ni with B atoms, it may be speculated that the small B atoms occupy sites between the large Ni atoms without changing the arrangement of the Ni atoms, similar as interstitial atoms in a crystal lattice. According to the Faber-Ziman formalism the total structure factor of a system where the B atoms are invisible ($b_B = 0$) is given by $c_{Ni}\,S_{NiNi} + c_B$ [see Eq. (3)]. In Fig. 3, this is compared with the structure factor of pure liquid Ni at similar temperature. Marked differences are visible, clearly indicating that alloying with B significantly changes the distribution of the Ni atoms. The second maximum of $c_{Ni}\,S_{NiNi} + c_B$ does not show the characteristic shoulder on the right-hand side that is found in $S(q)$ of pure liquid Ni and that is characteristic of a icosahedral short-range order (ISRO) [20]. Obviously, alloying with B destroys the ISRO that prevails in melts of pure Ni. Also, the Bhatia-Thornton partial structure S_{NN} that describes the TSRO of the melt significantly differs from that of pure liquid Ni, indicating a marked change of the TSRO due to the alloying with Ni.

Fourier-transforming the partial static structure factors provides the corresponding partial pair-correlation functions $g(r)$. They are depicted in the upper and lower panel of Fig. 4 for Faber-Ziman and Bhatia-Thornton formalisms, respectively. The first maximum of the $g_{NiB}(r)$ curve is higher and the area under this first maximum broader compared to the size of the first maxima and the corresponding areas under these maxima of $g_{NiNi}(r)$ and $g_{BB}(r)$, respectively. Consequently, heterogeneous nearest-neighbor pairs are preferred in the $Ni_{66.7}B_{33.3}$ melts. The same conclusion can be drawn from the fact that the Bhatia-Thornton pair-correlation function $g_{CC}(r)$ shows a pronounced minimum around 2 Å. The first maximum of

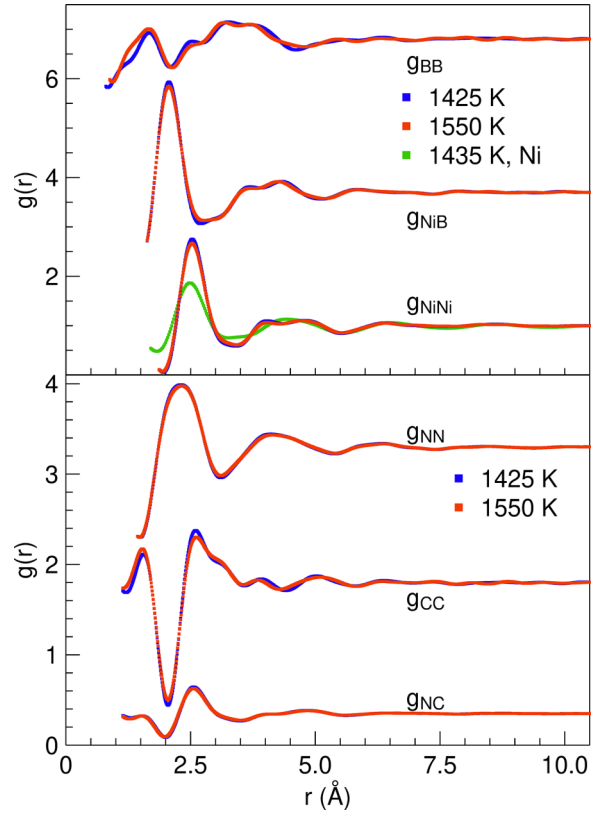

FIG. 4. Upper panel: Partial pair distribution functions $g(r)$ of liquid $Ni_{66.7}B_{33.3}$ calculated using the Faber-Ziman formalism [42] at 1425 K (blue symbols) and 1550 K (red symbols) versus the radius r. Green data points show $g(r)$ of pure Ni at 1435 K [20]. g_{NiB} is shifted up along the y axis by a value of 2.7, g_{BB} by 5.8. Lower panel: Partial pair distribution functions $g(r)$ of liquid $Ni_{66.7}B_{33.3}$ calculated using the Bhatia-Thornton formalism [43] at 1425 K (blue symbols) and 1550 K (red symbols) versus the radius r. The g_{NC} curve is shifted down along the y axis by a value of 0.65, g_{CC} and g_{NN} are shifted up by 0.8 and 2.3.

$g_{NiNi}(r)$ of $Ni_{66.7}B_{33.3}$ is sharper compared to that of pure Ni (green curve), which implies a broader distribution of Ni-Ni nearest-neighbor distances in pure Ni compared to the Ni-Ni nearest-neighbor distances in the $Ni_{66.7}B_{33.3}$ alloy.

Calculating the coordination numbers Z_{xy} and the nearest-neighbor distances d_{xy} with $x, y = \mathrm{Ni, B, N}$ give a more quantitative analysis of the SRO. The results are compiled in Table I at 1425 K and 1550 K. The coordination number of the density-density correlation $Z_{NN} \approx 12.7$ is slightly higher than that of pure Ni ($Z_{NiNi} = Z_{NN} = 12.3$) at $T = 1435$ K [20] (see Table I). In comparison, numbers of nearest neighbors of the Ni atoms ($Z_{NiNi} + Z_{BNi} \approx 14$) are larger compared to those of the B atoms ($Z_{BB} + Z_{NiB} \approx 8$). Hence, the SRO around the larger Ni atoms is considerably different in comparison to the SRO around the smaller B atoms. It should also be noted that the coordination number of Z_{BB} is only around 1. Hence, formation of direct nearest-neighbor pairs of B-B is not favored. It is remarkable that the second maximum of g_{BB} is larger than the first one, indicating that other B atoms are mainly located in the second coordination shell (or an even higher one) around a B atom. In the $Ni_{66.7}B_{33.3}$ alloy, the number

TABLE I. Coordination numbers Z_{xy} and nearest-neighbor distances d_{xy} in $Ni_{66.7}B_{33.3}$ and pure Ni [20] at different temperatures.

T (K)	Z_{NN}	Z_{NiNi}	Z_{NiB}	Z_{BNi}	Z_{BB}	d_{NN} (Å)	d_{NiNi} (Å)	d_{NiB} (Å)	d_{BB} (Å)	Ref.
$Ni_{66.7}B_{33.3}$:										
1425	12.7 ± 0.5	10.7 ± 0.5	7.1 ± 0.5	3.6 ± 0.5	0.9 ± 0.5	2.31 ± 0.02	2.53 ± 0.02	2.06 ± 0.02	1.67 ± 0.02	This paper
1550	12.6 ± 0.5	10.7 ± 0.5	7.1 ± 0.5	3.6 ± 0.5	1.0 ± 0.5	2.32 ± 0.02	2.53 ± 0.02	2.06 ± 0.02	1.66 ± 0.02	This paper
Pure Ni:										
1435	12.3 ± 0.5	$= Z_{NN}$				2.49 ± 0.02	$= d_{NN}$			[20]
1605	11.9 ± 0.5	$= Z_{NN}$				2.49 ± 0.02	$= d_{NN}$			[20]

of nearest neighbors of B atoms is $Z_{BB} + Z_{NiB} \approx 8$ and thus higher compared to the number of nearest neighbors of one B atom in pure liquid boron (around 6 [24]). Furthermore, $Z_{NiB} \approx 7$ (see Table I), which means that one B atom has about seven Ni atoms as direct nearest neighbors. Thus, clustering of B does not occur in the $Ni_{66.7}B_{33.3}$ melt as also indicated by the small Z_{BB}.

The interatomic distance d_{NiB} is smaller compared to $\frac{1}{2}(d_{NiNi} + d_{BB})$ at both temperatures 1425 K and 1550 K (see Table I), which is an indication for strong interactions between the atoms of Ni and B. Furthermore, d_{NiB} is also smaller than the sum of the Goldschmidt radii of Ni ($r_{Ni,GS} = 1.24$ Å [32]) and B ($r_{B,GS} = 0.98$ Å [32]), or the sum of the next-nearest-neighbor distances $\frac{1}{2}(d_{Ni} + d_B)$ in pure liquid Ni (2.49 Å) and B (1.78 Å) [20,24]. While in melts of pure Ni the nearest-neighbor distance $d_{NiNi} = 2.49$ Å corresponds to twice the Goldschmidt radius, the Ni-Ni nearest-neighbor distances in liquid $Ni_{66.7}B_{33.3}$ are larger by nearly 2%. Hence, alloying with B widens d_{NiNi}. Similar results have been found for liquid $Zr_{64}Ni_{36}$ [17], where the formation of heterogeneous Zr-Ni pairs is preferred.

To scrutinize the relation between the structure and dynamics in liquid $Ni_{66.7}B_{33.3}$ in more detail, we performed MCT [14] calculations by using the measured partial structure factors of $Ni_{66.7}B_{33.3}$ as input parameters. The number density of the melt for the calculation is taken from the measured liquid density [5]. A detailed description of the calculation can be found elsewhere [11,17]. The resulting self-diffusion coefficients using MCT calculations are depicted in Fig. 5. The Ni self-diffusion coefficient $D_{Ni}(\text{MCT}) = 1.18 \times 10^{-9}\,\text{m}^2\text{s}^{-1}$ at $T = 1425$ K predicted by the MCT and the previous experimentally determined Ni self-diffusion coefficient D_{Ni} by quasielastic neutron scattering $D_{Ni}(\text{QNS}) = (1.12 \pm 0.11) \times 10^{-9}\,\text{m}^2\text{s}^{-1}$ of $Ni_{66.7}B_{33.3}$ at $T = 1413$ K [5] show similar values in a similar temperature range (see Fig. 5). For $T = 1550$ K, the predicted Ni self-diffusion coefficient from the MCT calculation is about 1.5 times higher than that measured by QNS [5]. MCT invokes approximations that typically neglect relaxation processes that become important at lower temperatures. In particular, MCT predicts the diffusion coefficients to vanish at its critical point T_c, while the experimental values remain finite in this temperature range. We thus expect the MCT predictions to underestimate the experimental diffusion coefficients at lower temperatures. Nevertheless, it was shown that the temperature dependence of the diffusion coefficients can be reproduced in the case of Zr-Ni and Hf-Ni melts [17,19]. It seems that the deviation on the prediction of the temperature dependence in $Ni_{66.7}B_{33.3}$ is slightly larger than that in the case of Zr-Ni and Hf-Ni. Still, the ratio between the transport coefficients can be reliably predicted by MCT [14,16]. In particular, B self-diffusion is predicted to be about 1.8 times faster than the self-diffusion of Ni at $T = 1425$ K, and of about 1.6 times faster at $T = 1550$ K.

In addition to the self-diffusion coefficients of Ni and B, MCT can also give a prediction of the kinetic contribution to the interdiffusion coefficient D_{int}. In contrast to the self-diffusion coefficient, which describes the diffusive transport of one individual particle, the (chemical) interdiffusion coefficient is driven by the difference in chemical potentials, corresponding to the decay of concentration gradients at large scales [44]. The interdiffusion coefficient D_{int} can be described by the product of the kinetic contribution L (Onsager coefficient), which can be calculated for binary systems by using MCT calculations, and the thermodynamic factor Φ, $D_{int} = L\Phi$. For binary systems, Φ can be derived by thermodynamic calculations from the second-order derivative of the molar Gibbs free energy with respect to temperature and corresponding concentrations of the respective elements of the binary alloy [45]. For $Ni_{66.7}B_{33.3}$, the thermodynamic factor is given by Sun [46] and has a value of about 5.5. The thermodynamic factor can be also expressed by $1/S_{cc}(q \to 0)$. If we

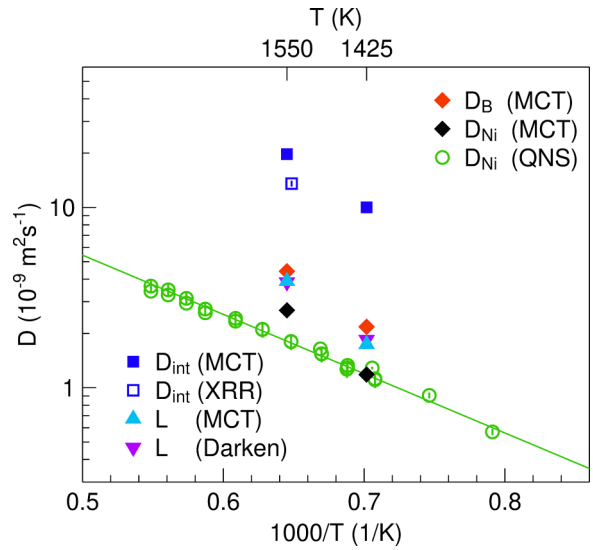

FIG. 5. Diffusion and Onsager coefficients, L, of $Ni_{66.7}B_{33.3}$ as a function of the inverse temperature. D_{int}(XRR) is measured using x-ray radiography (this paper). D_{Ni}(QNS) are Ni self-diffusion coefficients determined using QNS by Nell *et al.* [5]. The solid line is a corresponding fit of Arrhenius's law.

calculate Φ from $S_{cc}(q \to 0)$ for the binary system $Ni_{66.7}B_{33.3}$ (see Fig. 2), we preserve a value that is in agreement with the value of 5.5 of Sun [46] within the measurement uncertainties.

Using this thermodynamical factor ($\Phi = 5.5$ [46]) and the Onsager coefficient L (MCT) given by the MCT results in a value for the interdiffusion coefficient of D_{int} (MCT) $= 20.9 \times 10^{-9}\,\text{m}^2\text{s}^{-1}$ at 1550 K. The experimental determined interdiffusion coefficient using x-ray radiography (XRR) [47] at 1543 K is $(13.5 \pm 0.5) \times 10^{-9}\,\text{m}^2\text{s}^{-1}$. Thus, the ratio between the interdiffusion coefficient D_{int} (MCT) and the Ni self-diffusion coefficient D_{Ni} (MCT) from the MCT calculation agrees with the ratio between the experimental values D_{int} (XRR) and D_{Ni} (QNS) within the experimental uncertainties (see Fig. 5).

The empirical Darken equation links the self- and interdiffusion by [48]

$$D_{\text{int}} = \Phi L = \Phi(c_A D_B + c_B D_A), \tag{5}$$

where D_{int} is the interdiffusion coefficient and D_A and D_B are self-diffusion coefficients with the corresponding concentrations c_i $(i = A, B)$ of the respective elements A and B. Basically, here the Onsager coefficient L is expressed in terms of a linear combination of the two self-diffusion coefficients.

With the knowledge of the mobility of both constituents predicted by MCT, our results show that within measurement errors the Onsager coefficient can indeed be described using the Darken equation for $Ni_{66.7}B_{33.3}$ (see Fig. 5), indicating that the contribution of the cross correlation can be neglected. This is different compared to the case of the Zr-Ni alloy [16], where the Darken equation overestimates the interdiffusion coefficients and where thus the contribution of the cross correlation cannot be neglected [11,17].

IV. CONCLUSION

Through the techniques of neutron diffraction combined with isotopic substitution as well as x-ray diffraction and electrostatic levitation, we were able to obtain experimental data of high quality for the partial structure factors of liquid $Ni_{66.7}B_{33.3}$, which were used as input parameters for MCT calculations. This enables the prediction of dynamic quantities like, e.g., self- and interdiffusion coefficients, which are in good agreement with experimental results for liquid $Ni_{66.7}B_{33.3}$. The calculated B self-diffusion coefficients are twice as large as the Ni self-diffusion coefficients, indicating more decoupled atomic dynamics. Furthermore, we were able to show that the interdiffusion behavior in the $Ni_{66.7}B_{33.3}$ melt is well described by Darken's equation, indicating that the contribution of the cross correlation can be neglected.

ACKNOWLEDGMENTS

We thank B. Nowak, C. Reinerth, Z. Evenson, S. Szabó, P. Fopp, D. Zhao from our institute and P. Ramasamy and J. Wang from IFW Dresden for their help during experiments at ILL and ESRF. Furthermore, we thank E. Sondermann for a critical reading of the paper.

[1] H. Mehrer, *Diffusion in Solids: Fundamentals, Methods, Materials, Diffusion-Controlled Processes*, Springer Series in Solid-State Sciences (Springer, Berlin, 2007).

[2] A. Bartsch, K. Rätzke, A. Meyer, and F. Faupel, Dynamic arrest in multicomponent glass-forming alloys, Phys. Rev. Lett. **104**, 195901 (2010).

[3] C. C. Yuan, F. Yang, F. Kargl, D. Holland-Moritz, G. G. Simeoni, and A. Meyer, Atomic dynamics in Zr-(Co,Ni)-Al metallic glass-forming liquids, Phys. Rev. B **91**, 214203 (2015).

[4] J. Wilden, F. Yang, D. Holland-Moritz, S. Szabó, W. Lohstroh, B. Bochtler, R. Busch, and A. Meyer, Impact of sulfur on the melt dynamics of glass forming $Ti_{75}Ni_{25-x}S_x$, Appl. Phys. Lett. **117**, 013702 (2020).

[5] S. Nell, F. Yang, Z. Evenson, and A. Meyer, Viscous flow and self-diffusion in densely and loosely packed metallic melts, Phys. Rev. B **103**, 064206 (2021).

[6] F. Demmel, L. Hennet, S. Brassamin, D. R. Neuville, J. Kozaily, and M. M. Koza, Nickel self-diffusion in a liquid and undercooled NiSi alloy, Phys. Rev. B **94**, 014206 (2016).

[7] P. Protopapas, H. C. Andersen, and N. Parlee, Theory of transport in liquid metals. I. Calculation of self-diffusion coefficients, J. Comput. Phys. **59**, 15 (1973).

[8] G. Kaptay, A new theoretical equation for temperature dependent self-diffusion coefficients of pure liquid metals, Int. J. Mater. Res. **99**, 14 (2008).

[9] J. Brillo, A. I. Pommrich, and A. Meyer, Relation between self-diffusion and viscosity in dense liquids: New experimental results from electrostatic levitation, Phys. Rev. Lett. **107**, 165902 (2011).

[10] H. R. Schober, Reining in diffusion in dense liquids, Physics **4**, 80 (2011).

[11] F. Yang, P. Heintzmann, F. Kargl, K. Binder, B. Nowak, B. Schillinger, T. Voigtmann, and A. Meyer, Kinetics-dominated interdiffusion in metallic glass-forming liquids, Phys. Rev. B **98**, 064202 (2018).

[12] F. Demmel, Non-Arrhenius behaviour of nickel self-diffusion in liquid $Ni_{77}Si_{23}$, J. Phys.: Condens. Matter **34**, 395101 (2022).

[13] W. Götze, *Complex Dynamics of Glass-Forming Liquids: A Mode-Coupling Theory* (Oxford University Press, Oxford, 2009), Vol. 143.

[14] W. Götze and L. Sjogren, Relaxation processes in supercooled liquids, Rep. Prog. Phys. **55**, 241 (1992).

[15] W. Götze, Liquids, freezing and glass transition, in *Aspects of Structural Glass Transitions*, edited by J.-P. Hansen, D. Levesque, and J. Zinn-Justin (North-Holland, Amsterdam, 1991).

[16] T. Voigtmann, A. Meyer, D. Holland-Moritz, S. Stüber, T. Hansen, and T. Unruh, Atomic diffusion mechanisms in a binary metallic melt, Europhys. Lett. **82**, 66001 (2008).

[17] B. Nowak, D. Holland-Moritz, F. Yang, T. Voigtmann, T. Kordel, T. C. Hansen, and A. Meyer, Partial structure factors reveal atomic dynamics in metallic alloy melts, Phys. Rev. Mat. **1**, 025603 (2017).

[18] S. W. Basuki, F. Yang, E. Gill, K. Rätzke, A. Meyer, and F. Faupel, Atomic dynamics in Zr-based glass forming alloys near the liquidus temperature, Phys. Rev. B **95**, 024301 (2017).

[19] B. Nowak, D. Holland-Moritz, F. Yang, T. Voigtmann, Z. Evenson, T. C. Hansen, and A. Meyer, Effect of component substitution on the atomic dynamics in glass-forming binary metallic melts, Phys. Rev. B **96**, 054201 (2017).

[20] T. Schenk, D. Holland-Moritz, V. Simonet, R. Bellissent, and D. M. Herlach, Icosahedral short-range order in deeply undercooled metallic melts, Phys. Rev. Lett. **89**, 075507 (2002).

[21] D. Holland-Moritz, O. Heinen, R. Bellissent, and T. Schenk, Short-range order of stable and undercooled liquid titanium, Mater. Sci. Eng.: A **449-451**, 42 (2007).

[22] D. Holland-Moritz, F. Yang, T. C. Hansen, and F. Kargl, Chemical short-range order in liquid Ni-Cu, J. Phys.: Condens. Matter **35**, 465403 (2023).

[23] F. C. Frank, Supercooling of liquids, Proc. R. Soc. London A **215**, 43 (1952).

[24] S. Krishnan, S. Ansell, J. J. Felten, K. J. Volin, and D. L. Price, Structure of liquid boron, Phys. Rev. Lett. **81**, 586 (1998).

[25] H. Kimura, M. Watanabe, K. Izumi, T. Hibiya, D. Holland-Moritz, T. Schenk, K. R. Bauchspieß, S. Schneider, I. Egry, K. Funakoshi *et al.*, X-ray diffraction study of undercooled molten silicon, Appl. Phys. Lett. **78**, 604 (2001).

[26] H. Weis, D. Holland-Moritz, F. Kargl, F. Yang, T. Unruh, T. C. Hansen, J. Bednarčik, and A. Meyer, Short-range order and atomic diffusion in liquid Ge and $Si_{20}Ge_{80}$ investigated by neutron scattering and x-ray diffraction, Phys. Rev. B **104**, 134108 (2021).

[27] D. Holland-Moritz, B. Nowak, F. Yang, and A. Meyer, Structure and dynamics of glass-forming alloy melts investigated by application of levitation techniques, Pure Appl. Chem. **91**, 895 (2019).

[28] L. Huang, C. Z. Wang, S. G. Hao, M. J. Kramer, and K. M. Ho, Atomic size and chemical effects on the local order of Zr_2M (M = Co, Ni, Cu, and Ag) binary liquids, Phys. Rev. B **81**, 014108 (2010).

[29] P. Gaskell, A new structural model for transition metal–metalloid glasses, Nature (London) **276**, 484 (1978).

[30] P. F. Guan, T. Fujita, A. Hirata, Y. H. Liu, and M. W. Chen, Structural origins of the excellent glass forming ability of $Pd_{40}Ni_{40}P_{20}$, Phys. Rev. Lett. **108**, 175501 (2012).

[31] C. Yuan, F. Yang, X. Xi, C. Shi, D. Holland-Moritz, M. Li, F. Hu, B. Shen, X. Wang, A. Meyer, and W. Wang, Impact of hybridization on metallic-glass formation and design, Mater. Today **32**, 26 (2020).

[32] L. Pauling, Atomic radii and interatomic distances in metals, J. Am. Chem. Soc. **69**, 542 (1947).

[33] T. C. Hansen, P. F. Henry, H. E. Fischer, J. Torregrossa, and P. Convert, The D20 instrument at the ILL: a versatile high-intensity two-axis neutron diffractometer, Meas. Sci. Technol. **19**, 034001 (2008).

[34] A. J. Dianoux and G. H. Lander, *Neutron Data Booklet* (Institut Laue Langevin in cooperation with Old City Publishing, Philadelphia, 2003).

[35] T. Kordel, D. Holland-Moritz, F. Yang, J. Peters, T. Unruh, T. Hansen, and A. Meyer, Neutron scattering experiments on liquid droplets using electrostatic levitation, Phys. Rev. B **83**, 104205 (2011).

[36] D. Holland-Moritz, T. Schenk, P. Convert, T. Hansen, and D. Herlach, Electromagnetic levitation apparatus for diffraction investigations on the short-range order of undercooled metallic melts, Meas. Sci. Technol. **16**, 372 (2005).

[37] G. B. M. Vaughan, R. Baker, R. Barret, J. Bonnefoy, T. Buslaps, S. Checchia, D. Duran, F. Fihman, P. Got, J. Kieffer, S. A. J. Kimber, K. Martel, C. Morawe, D. Mottin, E. Papillon, S. Petitdemange, A. Vamvakeros, J.-P. Vieux, and M. Di Michiel, ID15A at the ESRF—a beamline for high speed *operando* x-ray diffraction, diffraction tomography and total scattering, J. Synchrotron Radiat. **27**, 515 (2020).

[38] G. Ashiotis, A. Deschildre, Z. Nawaz, J. P. Wright, D. Karkoulis, F. E. Picca, and J. Kieffer, The fast azimuthal integration Python library: *pyFAI*, J. Appl. Cryst. **48**, 510 (2015).

[39] X. Qiu, J. W. Thompson, and S. J. Billinge, *PDFgetX2*: A GUI-driven program to obtain the pair distribution function from x-ray powder diffraction data, J. Appl. Crystallogr. **37**, 678 (2004).

[40] W. Götze and T. Voigtmann, Effect of composition changes on the structural relaxation of a binary mixture, Phys. Rev. E **67**, 021502 (2003).

[41] R. Ushio and O. Ogawa, Activities of boron in the binary Ni-B and the ternary Co-Fe-B melts, Metall. Trans. B **22**, 47 (1991).

[42] T. E. Faber and J. M. Ziman, A theory of the electrical properties of liquid metals, Philos. Mag. **11**, 153 (1965).

[43] A. B. Bhatia and D. E. Thornton, Structural aspects of the electrical resistivity of binary alloys, Phys. Rev. B **2**, 3004 (1970).

[44] J.-P. Hansen and I. R. McDonald, *Theory of Simple Liquids* (Elsevier, London, 1990).

[45] Y. A. Chang and W. A. Oates, *Materials Thermodynamics* (John Wiley & Sons, New Jersey, 2010), p. 292.

[46] W.-H. Sun, Y. Du, Y. Kong, H.-H. Xu, W. Xiong, and S.-H. Liu, Reassessment of the Ni-B system supported by key experiments and first-principles calculation, Int. J. Mater. Res. **100**, 59 (2009).

[47] E. Sondermann, F. Kargl, and A. Meyer, Influence of cross correlations on interdiffusion in Al-rich Al-Ni melts, Phys. Rev. B **93**, 184201 (2016).

[48] L. S. Darken, Diffusion, mobility and their interrelation through free energy in binary metallic systems, Trans. Aime **175**, 184 (1948).